A continuous shape sensitivity equation method for unsteady laminar flows

Ilinca, F.; Pelletier, D.

Publisher's version / Version de l'éditeur:
https://doi.org/10.1080/10618560701649952
International Journal of Computational Fluid Dynamics, 21, 7-8, pp. 255-266, 2007-08-01

International Journal of Computational Fluid Dynamics, Vol. 21, Nos. 7–8, August–September 2007, 255–266

A continuous shape sensitivity equation method for unsteady laminar flows

F. ILINCA†* and D. PELLETIER‡

†Industrial Materials Institute, National Research Council, Boucherville (Québec), Canada J4B 6Y4
‡Mechanical Engineering Department, École Polytechnique de Montréal, Montréal (Québec), Canada H3C 3A7

(Received 27 November 2006; accepted 19 March 2007)

This paper presents the application of a general shape sensitivity equation method (SEM) to unsteady laminar flows. The formulation accounts for complex parameter dependence and is suitable for a wide range of problems. The flow and sensitivity equations are solved on 3D meshes using a Streamline-Upwind Petrov Galerkin (SUPG) finite element method. In the case of shape parameters, boundary conditions for sensitivities depend on the flow gradient at the boundary. Therefore, an accurate recovery of solution gradients is crucial to the success of shape sensitivity computations. In this work, solution gradients at boundary points are extracted using the Finite Node Displacement (FiND) method on which the finite element discretization is enriched locally via the insertion of nodes close to the boundary points. The normal derivative of the solution is then determined using finite differences. This approach to evaluate shape sensitivity boundary conditions is embedded in the continuous SEM. The methodology is applied to the flow past a cylinder in ground proximity. First, the proposed method is verified on a steady state problem. The computed sensitivity is compared to the actual change in the solution when a small perturbation is imposed to the shape parameter. Then, the study investigates the ability of the SEM to anticipate the unsteady flow response to changes in the ground to cylinder gap. A reduction of the gap causes damping of the vortex shedding while an increase amplifies the unsteadiness.

Keywords: Shape Sensitivity; Flow Control; Finite elements; Unsteady flows

1. Introduction

Sensitivity analysis is a powerful tool in computational fluid dynamics. A sensitivity, (the derivative of the solution with respect to a parameter) indicates how a dependent variable reacts to variations in a design parameter. Sensitivity information finds many uses ranging from driving optimization algorithms, to fast evaluation of flows on nearby geometries or to computing uncertainty estimates of the solution. Sensitivities also find applications in flow control due to their ability to indicate how the flow responds to changes in design parameters. In all cases cost-effectiveness is achieved because sensitivities are obtained at a fraction of the cost of computing the flow.

Sensitivity analysis is a more advanced field in solid mechanics than in fluid dynamics. Indeed, textbooks have been written on sensitivity analysis of structures (Haug *et al.* 1986, Hien and Kleiber 1997). To our knowledge, there is only one book on sensitivity analysis of flow problems (Stanley and Stewart 2001). It is recent and more specialized than structural mechanics books. Gunzburger (2002) discusses sensitivity analysis in the context of flow control and optimization.

There are several means of computing flow sensitivities: finite differences of flow solutions, the complex step method (Martins *et al.* 2003, Lu and Sagaut 2006), automatic differentiation (Putko *et al.* 2001), and sensitivity equation methods (SEM; Borggaard and Burns 1997, Stanley and Stewart 2001, Turgeon *et al.* 2002). The finite difference approach is a well-known technique of estimating derivatives. It is based on the following approximation of the derivative of a function f:

$$\frac{\mathrm{d}f}{\mathrm{d}x} \approx \frac{f(x+h) - f(x)}{h} \tag{1}$$

The truncation error is $\mathcal{O}(h)$, and thus this is a first-order approximation of the derivative. Note that in our case, a full Navier–Stokes simulation must be performed for each evaluation of f. Higher-order finite difference stencils can be derived, at the cost of additional flow evaluations. This option is thus costly because the problem must be

*Corresponding author. Email: florin.ilinca@cnrc-nrc.gc.ca

International Journal of Computational Fluid Dynamics
ISSN 1061-8562 print/ISSN 1029-0257 online © 2007 Government of Canada
http://www.tandf.co.uk/journals
DOI: 10.1080/10618560701649952

solved for two or more values of each parameter of interest. For example, if **a** represents a vector of 10 parameters with respect to which we need to compute the flow sensitivity, then 11 flow evaluations are required; one for the baseline values of $\mathbf{a}_0$, and one per perturbation for each of the 10 parameters. In the case of a shape parameter, further technical problems arise because non matching meshes are obtained for different values of the shape parameter.

The complex-step method as a computational tool for evaluating derivatives was demonstrated by Lyness and Moler (1967). It is a very effective technique based on the following properties of complex numbers. Consider a function, $f = u + iv$, of the complex variable, $z = x + iy$. If f is analytic, then the Cauchy–Riemann equations apply

$$\frac{\partial u}{\partial x} = \frac{\partial v}{\partial y} \tag{2}$$

$$\frac{\partial u}{\partial y} = \frac{\partial v}{\partial x} \tag{3}$$

The first condition can be used to write the following approximation

$$\frac{\partial u}{\partial x} = \lim_{h \to 0} \frac{v(x + i(y + h)) - v(x + iy)}{h} \tag{4}$$

where h is a real number. We can set $y = 0$, $u(x) = f(x)$ and $v(x) = 0$ because the original problem involved only real variables so that equation (4) can then be rewritten as

$$\frac{\partial f}{\partial x} = \lim_{h \to 0} \frac{\Im[f(x + ih)]}{h} \tag{5}$$

For a small discrete h, this can be approximated by

$$\frac{\partial f}{\partial x} \approx \frac{\Im[f(x + ih)]}{h} \tag{6}$$

This complex-step derivative approximation is very robust and is not subject to subtractive cancellation errors, since it does not involve a difference operation. However, it requires a complete rewrite of the software in complex variables. While this can be automated, it has a significant impact on performance.

Automatic differentiation (also known as algorithmic differentiation or computational differentiation) is a well established method for estimating derivatives. The method is based on the application of the chain rule of differentiation to each operation in the program simulating the flow. It is equivalent to differentiating the discrete equations to generate a system of equations for the discrete sensitivities. It is powerful because it automatically generates the code for calculating sensitivities (Griewank 2000). In many cases, implementation requires human intervention to ensure efficiency of the code. Automatic differentiation for first-order flow sensitivities is discussed by Sherman *et al.* (1996) and Putko *et al.* (2001).

Approaches to calculating sensitivities also differ depending on the order of the operations of approximation and differentiation. In the *discrete* sensitivity equation approach, the total derivative of the flow approximation with respect to the parameter is calculated (Haug *et al.* 1986), whereas in the *continuous* SEM one differentiates the continuum equations to yield differential equations for the continuous sensitivities (Borggaard and Burns 1997). See Hien and Kleiber (1997) for a discussion of the two approaches. We have adopted the latter approach.

Continuous SEMs may be found in Borggaard and Burns (1997), Godfrey and Cliff (1998, 2001), Limache (2000) and Turgeon *et al.* (2001) for aerodynamics applications. Application to heat conduction is reported by Blackwell *et al.* (1998). Sensitivities for incompressible flows with heat transfer may be found in several references (Turgeon *et al.* 2000, 2002, 2003). Sensitivity analysis for turbulence models is detailed in the works by Godfrey and Cliff (2001) and Turgeon *et al.* (2004). Solution of the sensitivity equations for the transient incompressible flow of non-Newtonian fluids is presented by Ilinca *et al.* (2005). A wide variety of flow regimes were treated by the authors, Turgeon *et al.* (2000, 2002, 2003, 2004). This body of work has shown that, sensitivities provide an enriched basis of information on which to develop an understanding of complex flow problems.

The work presented here is an extension to shape parameters of the unsteady SEM by Hristova *et al.* (2006) and Ilinca *et al.* (2007) for laminar flows. A methodology for computing the continuous shape sensitivities is presented by Duvigneau and Pelletier (2005). For shape parameters, first derivatives of the solution appear in Dirichlet boundary conditions for the sensitivity variable. Second derivatives appear in the case of Neumann boundary conditions. The observed lower accuracy of boundary derivatives seem to occur because the derivatives extracted by most methods are not compatible or consistent with the solution field at or near the boundary. Duvigneau and Pelletier (2006) have recently proposed a Taylor series based constrained least squares procedure to extract high accuracy boundary derivatives that are compatible with the imposed Dirichlet conditions. However, the cost of the Taylor series least-squares method is too high for practical 3D applications.

In this paper, high accuracy nodal derivatives of the finite element solution are computed using the Finite Node Displacement (FiND) method, which was proposed by Ilinca and Pelletier (2007) for scalar convection-diffusion equations. For boundary nodes this approach is based on inserting an additional mesh node close to the boundary point, and on solving a small local problem on the patch of elements surrounding the node. The only unknown to this problem is the value of the solution at the additional point. The location of the additional point is given by applying a finite displacement to boundary nodes in the direction normal to the boundary and towards the interior of

the domain. A finite difference between the solution at the additional point and that at the boundary node yields the normal derivative at the boundary. The method provides nodal gradients that are consistent with the auxiliary fluxes (Hughes *et al.* 2000) on Dirichlet boundary nodes. Boundary nodal derivatives computed with this new method are much more accurate than those provided by the superconvergent patch recovery technique of Zienkiewicz and Zhu (1992).

The paper is organized as follows. First, we present the equations describing time-dependent laminar flow along with their boundary and initial conditions. The shape sensitivity equations and their boundary/initial conditions are then described in detail. The recovery of the solution gradient at the boundary is then presented. The approach is applied to the flow around a circular cylinder in ground proximity. The methodology and its finite element solver are first verified on a steady state problem. The paper then focuses on unsteady flows and the ability of sensitivities to anticipate important changes in the flow response due to shape changes. We use the example of vortex shedding behind a cylinder in ground proximity. We study to what extent sensitivities can predict amplification/damping of vortex shedding when the ground to cylinder gap varies. The paper ends with conclusions.

2. Flow equations

The flow regime of interest is modelled by the momentum and continuity equations:

$$\rho\left(\frac{\partial \mathbf{u}}{\partial t}+\mathbf{u}\cdot\nabla\mathbf{u}\right)=-\nabla p+\mathbf{f}+\nabla\cdot[2\mu\gamma(\mathbf{u})] \tag{7}$$

$$\nabla\cdot\mathbf{u}=0 \tag{8}$$

where ρ is the density, $\mathbf{u}$ is the velocity, p is the pressure, μ is the viscosity, t represents time, $\mathbf{f}$ is a body force and $\gamma(\mathbf{u})=(\nabla\mathbf{u}+\nabla\mathbf{u}^{\mathrm{T}})/\mathbf{2}$ is the strain rate tensor.

2.1 Initial and boundary conditions

The above system is closed with a proper set of initial conditions

$$\mathbf{u}(\mathbf{x},t=0)=\mathbf{U}_0(\mathbf{x})\ \text{ in }\ \Omega \tag{9}$$

and Dirichlet and Neumann boundary conditions

$$\mathbf{u}(\mathbf{x},t)=\mathbf{U}_{\mathrm{D}}(\mathbf{x},t)\ \text{ on }\ \Gamma_{\mathrm{D}} \tag{10}$$

$$\mathbf{t}=[-p\mathbf{I}+2\mu\gamma(\mathbf{u})]\cdot\hat{\mathbf{n}}=\mathbf{F}^{\mathrm{N}}\ \text{ on }\ \Gamma_{\mathrm{N}} \tag{11}$$

where $\mathbf{U}_{\mathrm{D}}$ is the value of the velocity imposed on the boundary Γ_{D}, $\mathbf{I}$ is the identity tensor, and $\mathbf{F}^{\mathrm{N}}$ is the imposed boundary value of the surface traction force $\mathbf{t}$.

2.2 Finite element solution

The flow equations are solved by a finite element method on 3D meshes. For simplicity, robustness and cost effectiveness of the simulations we use equal order interpolation for velocity and pressure (P1–P1 tetrahedral elements) that need stabilization terms to avoid velocity–pressure decoupling (Hughes *et al.* 1986, 1989, Franca and Frey 1992). Stabilization can also avoid spurious oscillations in convection-dominated flows. In this work a Streamline-Upwind Petrov Galerkin (SUPG) finite element method is used. Time is discretized by an implicit Euler scheme.

The SUPG variational formulation of the momentum-continuity equations is (Franca and Frey 1992, Ilinca *et al.* 2000):

$$\begin{aligned}&\int_\Omega\left\{\rho\left(\frac{\partial\mathbf{u}}{\partial t}+\mathbf{u}\cdot\nabla\mathbf{u}\right)-\mathbf{f}\right\}\mathbf{v}\mathrm{d}\Omega-\int_\Omega p(\nabla\cdot\mathbf{v})\mathrm{d}\Omega\\&+\int_\Omega 2\mu\gamma(\mathbf{u}):\gamma(\mathbf{v})\mathrm{d}\Omega\ +\sum_K\int_{\Omega_K}\left\{\rho\left(\frac{\partial\mathbf{u}}{\partial t}+\mathbf{u}\cdot\nabla\mathbf{u}\right)\right.\\&\left.+\nabla p-\nabla[2\mu\gamma(\mathbf{u})]-\mathbf{f}\right\}\tau_u(\rho\mathbf{u}\cdot\nabla\mathbf{v})\mathrm{d}\Omega_K\\&+\sum_K\int_{\Omega_K}(\nabla\cdot\mathbf{u})\delta(\nabla\cdot\mathbf{v})\mathrm{d}\Omega_K=\int_{\Gamma_{\mathrm{N}}}\mathbf{F}^{\mathrm{N}}\mathbf{v}\mathrm{d}\Gamma_{\mathrm{N}}\end{aligned} \tag{12}$$

$$\begin{aligned}&\int_\Omega(\nabla\cdot\mathbf{u})q\mathrm{d}\Omega+\sum_K\int_{\Omega_K}\left\{\rho\left(\frac{\partial\mathbf{u}}{\partial t}+\mathbf{u}\cdot\nabla\mathbf{u}\right)\right.\\&\left.+\nabla p-\nabla[2\mu\gamma(\mathbf{u})]-\mathbf{f}\right\}\tau_u\nabla q\mathrm{d}\Omega_K=0\end{aligned} \tag{13}$$

where $\mathbf{v}$ and q denote the velocity and pressure test functions respectively and Ω_K denotes the volume of element K. The integrals over the entire domain identify the Galerkin contribution, while the stabilization terms are integrated only on the element interiors (i.e. terms in the summations). The stabilization parameters τ_u and δ are defined as (Tezduyar *et al.* 1990, Ilinca *et al.* 2000):

$$\tau_u=\left[\left(\frac{2\rho}{\Delta t}\right)^2+\left(\frac{2\rho|\mathbf{u}|}{h_K}\right)^2+\left(\frac{4\mu}{m_k h_K^2}\right)^2\right]^{-1/2} \tag{14}$$

$$\delta=\frac{h_K^2}{2\tau_u} \tag{15}$$

Here Δt is the time step, h_K is the size of the element K and m_k is a coefficient set to 1/3 for linear elements (Tezduyar *et al.* 1990, Franca and Frey 1992).

3. Sensitivity equations

The continuous sensitivity equations (CSE) are derived formally by implicit differentiation of the flow equations (7) and (8) with respect to parameter a. We treat the variable $\mathbf{u}$ as a function of space, time and of the parameter a. This dependence is denoted by $\mathbf{u}(\mathbf{x},t;a)$. Defining the flow sensitivities as the partial derivatives $\mathbf{s_u} = \partial\mathbf{u}/\partial a$ and $s_p = \partial p/\partial a$, and denoting the total derivatives of the fluid properties and other flow parameters by a ($'$), differentiation of equations (7) and (8) yields

$$\rho'\left(\frac{\partial \mathbf{u}}{\partial t}+\mathbf{u}\cdot\nabla\mathbf{u}\right)+\rho\left(\frac{\partial \mathbf{s_u}}{\partial t}+\mathbf{u}\cdot\nabla\mathbf{s_u}+\mathbf{s_u}\cdot\nabla\mathbf{u}\right)$$
$$=-\nabla s_p+\mathbf{f}' \quad +\nabla\left[\mu'(\nabla\mathbf{u}+(\nabla\mathbf{u})^{\mathrm{T}})+\mu(\nabla\mathbf{s_u}+(\nabla\mathbf{s_u})^{\mathrm{T}})\right] \tag{16}$$

$$\nabla\cdot\mathbf{s_u}=0 \tag{17}$$

3.1 Initial and boundary conditions

Initial conditions for the sensitivity equations are obtained by implicit differentiation of equation (9)

$$\mathbf{s_u}(\mathbf{x},t=0)=\frac{\partial \mathbf{U}_0}{\partial a}(\mathbf{x}) \quad \text{in } \Omega \tag{18}$$

Dirichlet and Neumann boundary condition are obtained in a similar manner. However, if a is a shape parameter, the position of the boundary is also parameter dependent. Therefore, the differentiation must account for the dependence on a of both the boundary data and the boundary location. For Dirichlet boundary conditions we require that the material derivative of the flow velocity be equal to that of $\mathbf{U}_{\mathrm{D}}$:

$$\frac{\mathrm{D}\mathbf{u}}{\mathrm{D}a}=\frac{\mathrm{D}\mathbf{U}_{\mathrm{D}}}{\mathrm{D}a} \quad \text{on } \Gamma_{\mathrm{D}} \tag{19}$$

$$\frac{\partial \mathbf{u}}{\partial a}+\nabla\mathbf{u}\frac{\partial \mathbf{x}}{\partial a}=\frac{\partial \mathbf{U}_{\mathrm{D}}}{\partial a} \quad \text{on } \Gamma_{\mathrm{D}} \tag{20}$$

thus we get

$$\mathbf{s_u}=\frac{\partial \mathbf{U}_{\mathrm{D}}}{\partial a}-\nabla\mathbf{u}\frac{\partial \mathbf{x}}{\partial a} \quad \text{on } \Gamma_{\mathrm{D}} \tag{21}$$

Similar reasoning leads to the following Neumann condition:

$$[-s_p\mathbf{I}+2(\mu\gamma(\mathbf{s_u})+\mu'\gamma(\mathbf{u}))]\hat{\mathbf{n}}$$
$$=\frac{\partial \mathbf{F}^{\mathrm{N}}}{\partial a}-\left\{\nabla[-p\mathbf{I}+2\mu\gamma(\mathbf{u})]\frac{\partial \mathbf{x}}{\partial a}\right\}\cdot\hat{\mathbf{n}}$$
$$-[-p\mathbf{I}+2\mu\gamma(\mathbf{u})]\frac{\partial \hat{\mathbf{n}}}{\partial a} \quad \text{on } \Gamma_{\mathrm{N}} \tag{22}$$

Equation (21) shows that the flow gradients at the wall are needed to evaluate Dirichlet boundary conditions for the sensitivities. Equation (22) reveals that second derivatives of velocity are needed in the case of a Neumann boundary condition for a shape parameter. This introduces numerical difficulties when solving CSE, since approximate boundary conditions are used. In this work only the Dirichlet boundary conditions are dependent on the shape parameter. Sensitivity boundary conditions are evaluated by extracting the normal derivatives from local finite element problems on patches of elements surrounding the boundary nodes (see Section 3.4).

3.2 Finite element solution of sensitivity equations

In theory the CSE can be solved by any numerical method. In practice, it is convenient and cost effective to use the same finite element method for the flow and the CSE. Indeed, we note that the CSE amounts to a Newton linearization of the Navier–Stokes equations. Thus, if one uses Newton's method for solving the finite element equations for the flow, the flow sensitivity equations will have the same finite element matrix. Only the right hand side will differ. This results in substantial savings since the matrix of the sensitivities need not be recomputed. In practice the solution for the sensitivity with respect to one parameter is obtained at approximately 10% of the cost of solving the flow equations.

Here the sensitivity equations are solved by the same SUPG method used for flow equations. For simplicity we present here the finite element method in the case of constant properties flows:

$$\int_\Omega\left\{\rho\left(\frac{\partial \mathbf{s_u}}{\partial t}+\mathbf{u}\cdot\nabla\mathbf{s_u}+\mathbf{s_u}\cdot\nabla\mathbf{u}\right)-\mathbf{f}'\right\}\mathbf{v}\mathrm{d}\Omega$$
$$-\int_\Omega s_p(\nabla\cdot\mathbf{v})\mathrm{d}\Omega+\int_\Omega 2\mu\gamma(\mathbf{s_u}):\gamma(\mathbf{v})\mathrm{d}\Omega$$
$$+\sum_K\int_{\Omega_K}\left\{\rho\left(\frac{\partial \mathbf{s_u}}{\partial t}+\mathbf{u}\cdot\nabla\mathbf{s_u}+\mathbf{s_u}\cdot\nabla\mathbf{u}\right)+\nabla s_p\right.$$
$$\left.-\nabla[2\mu\gamma(\mathbf{s_u})]-\mathbf{f}'\right\}\tau_u(\rho\mathbf{u}\cdot\nabla\mathbf{v})\mathrm{d}\Omega_K$$
$$+\sum_K\int_{\Omega_K}(\nabla\cdot\mathbf{s_u})\delta(\nabla\cdot\mathbf{v})\mathrm{d}\Omega_K=\int_{\Gamma_{\mathrm{N}}}\frac{\partial \mathbf{F}^{\mathrm{N}}}{\partial a}\mathbf{v}\mathrm{d}\Gamma_{\mathrm{N}} \tag{23}$$

$$\int_\Omega(\nabla\cdot\mathbf{s_u})q\mathrm{d}\Omega+\sum_K\int_{\Omega_K}\left\{\rho\left(\frac{\partial \mathbf{s_u}}{\partial t}+\mathbf{u}\cdot\nabla\mathbf{s_u}+\mathbf{s_u}\cdot\nabla\mathbf{u}\right)\right.$$
$$\left.+\nabla s_p-\nabla[2\mu\gamma(\mathbf{s_u})]-\boldsymbol{f}'\right\}\tau_u\nabla q\mathrm{d}\Omega_K=0 \tag{24}$$

The integrals over the entire domain represent the Galerkin contribution, whereas the integrals over the

element interiors represent the SUPG stabilization terms for the sensitivity equations.

3.3 Normal component of velocity sensitivity at the boundary

For incompressible flows, the boundary conditions for the sensitivities of the velocity satisfy strict relationships where Dirichlet boundary conditions are imposed on the flow. Without loss of generality we restrict ourselves to the case of homogeneous Dirichlet conditions. In this specific case, and for shape parameters, the sensitivity of the velocity is always tangent to the surface. To prove this we begin with the equation (21) for $U_D = 0$:

$$\mathbf{s_u} = -\nabla \mathbf{u} \frac{\partial \mathbf{x}}{\partial a} \tag{25}$$

which has the following scalar components:

$$s_u = -\left[\frac{\partial u}{\partial x}\frac{\partial x}{\partial a} + \frac{\partial u}{\partial y}\frac{\partial y}{\partial a} + \frac{\partial u}{\partial z}\frac{\partial z}{\partial a}\right] \tag{26}$$

$$s_v = -\left[\frac{\partial v}{\partial x}\frac{\partial x}{\partial a} + \frac{\partial v}{\partial y}\frac{\partial y}{\partial a} + \frac{\partial v}{\partial z}\frac{\partial z}{\partial a}\right] \tag{27}$$

$$s_w = -\left[\frac{\partial w}{\partial x}\frac{\partial x}{\partial a} + \frac{\partial w}{\partial y}\frac{\partial y}{\partial a} + \frac{\partial w}{\partial z}\frac{\partial z}{\partial a}\right] \tag{28}$$

The normal component of the velocity sensitivity is given by:

$$\begin{aligned} -\mathbf{s_u}\cdot\hat{\mathbf{n}} = &\left[\frac{\partial u}{\partial x}n_x + \frac{\partial v}{\partial x}n_y + \frac{\partial w}{\partial x}n_z\right]\frac{\partial x}{\partial a} \\ &+ \left[\frac{\partial u}{\partial y}n_x + \frac{\partial v}{\partial y}n_y + \frac{\partial w}{\partial y}n_z\right]\frac{\partial y}{\partial a} \\ &+ \left[\frac{\partial u}{\partial z}n_x + \frac{\partial v}{\partial z}n_y + \frac{\partial w}{\partial z}n_z\right]\frac{\partial z}{\partial a} \end{aligned} \tag{29}$$

where $\hat{\mathbf{n}} = (n_x, n_y, n_z)$ is the outward unit normal to the boundary and the derivatives of the velocity satisfy the incompressibility condition (8):

$$\frac{\partial u}{\partial x} + \frac{\partial v}{\partial y} + \frac{\partial w}{\partial z} = 0 \tag{30}$$

Consider now the first bracket on the right hand-side of (29) in which we replace $\partial u/\partial x$ by $-((\partial v/\partial y) + (\partial w/\partial z))$ using (30), to obtain:

$$\begin{aligned} \frac{\partial u}{\partial x}n_x + \frac{\partial v}{\partial x}n_y + \frac{\partial w}{\partial x}n_z = &\left(\frac{\partial v}{\partial x}n_y - \frac{\partial v}{\partial y}n_x\right) \\ &+ \left(\frac{\partial w}{\partial x}n_z - \frac{\partial w}{\partial z}n_x\right) \end{aligned} \tag{31}$$

Because $\mathbf{u}$ vanishes on the boundary, the derivative of the velocity in any tangential direction $\hat{\mathbf{t}}$ to the boundary is zero: $\nabla\mathbf{u}\cdot\hat{\mathbf{t}} = 0$. Thus, the two terms on the right hand-side of equation (31) vanish, because $(n_y, -n_x, 0)$ and $(n_z, 0, -n_x)$ define two tangent directions and the derivatives of v and w along these directions are zero. A similar treatment applies to the other two brackets of equation (29) so that we obtain:

$$\mathbf{s_u}\cdot\hat{\mathbf{n}} = 0 \tag{32}$$

indicating that the normal component of the velocity sensitivity is zero at the boundary. This is a very useful tool for assessing the accuracy of the approximate boundary conditions for the sensitivities.

In the case of a non-homogeneous Dirichlet boundary condition the normal component of the velocity sensitivity is non-zero but it can be determined in terms of the velocity boundary condition. In either case, the normal component is known and can be used as an error estimate to test the accuracy of the computed sensitivity boundary conditions.

3.4 Evaluation of velocity gradient at Dirichlet boundary nodes

The accuracy of the shape sensitivity solution depends mainly on our ability to recover accurate flow derivatives at the boundary. We apply here the FiND method proposed by Ilinca and Pelletier (2007) for convection-diffusion equations. In this work the procedure is extended to the estimation of velocity gradients on Dirichlet boundary nodes. The proposed approach improves the accuracy of the nodal flow derivatives over previous recovery techniques. For simplicity we restrict ourselves to the case where Dirichlet conditions are specified on the parameter dependent boundary segment. For this case flow gradients at the wall are needed to evaluate boundary conditions via equation (21). To improve accuracy we express the derivatives in the normal and tangential directions as follows

$$\frac{\partial \mathbf{u}}{\partial n} = \frac{\partial \mathbf{u}}{\partial x}n_x + \frac{\partial \mathbf{u}}{\partial y}n_y + \frac{\partial \mathbf{u}}{\partial z}n_z \tag{33}$$

$$\frac{\partial \mathbf{u}}{\partial t_1} = \frac{\partial \mathbf{u}}{\partial x}t_{1x} + \frac{\partial \mathbf{u}}{\partial y}t_{1y} + \frac{\partial \mathbf{u}}{\partial z}t_{1z} \tag{34}$$

$$\frac{\partial \mathbf{u}}{\partial t_2} = \frac{\partial \mathbf{u}}{\partial x}t_{2x} + \frac{\partial \mathbf{u}}{\partial y}t_{2y} + \frac{\partial \mathbf{u}}{\partial z}t_{2z} \tag{35}$$

where $\hat{\mathbf{n}}$ is the boundary outward unit normal and $\hat{\mathbf{t}}_1 = (t_{1x}, t_{1y}, t_{1z})$, $\hat{\mathbf{t}}_2 = (t_{2x}, t_{2y}, t_{2z})$ are two orthogonal unit vectors tangent to the boundary. On boundaries with homogeneous Dirichlet conditions the tangential derivatives are zero, $\partial\mathbf{u}/\partial t_1 = 0$, $\partial\mathbf{u}/\partial t_2 = 0$, and we need only determine the velocity derivative in normal direction.

The derivative of $\mathbf{u}$ in the direction $\hat{\mathbf{n}}$, the nodal normal to the boundary, is given by

$$\frac{\partial \mathbf{u}}{\partial n}(\mathbf{x}_P) = -\lim_{\delta x_n \to 0} \frac{\mathbf{u}(\mathbf{x}_P + \delta \mathbf{x}_n) - \mathbf{u}(\mathbf{x}_P)}{\delta x_n} \tag{36}$$

where x_P is the coordinate of the boundary node P where the normal derivative is computed and $\delta \mathbf{x}_n = -\delta x_n \hat{\mathbf{n}}$ is a displacement of magnitude δx_n in the normal direction towards the interior of the domain (the minus sign appears because the finite element normal vector $\hat{\mathbf{n}}$ is the unit outward normal). To extract the normal derivative we must first determine the solution $\mathbf{u}(\mathbf{x}_P + \delta \mathbf{x}_n)$ in equation (36). To this end, an additional point P' is inserted in the mesh at $\mathbf{x}_P + \delta \mathbf{x}_n$. A local problem is solved for the solution at P'.

The procedure is illustrated in figure 1 for 2D problems and linear triangular elements. Integration of the finite element equation for node P is performed in the two-element patch Ω_P, and Γ_P denotes the portion of the patch boundary $\partial\Omega_P$ coinciding with the domain boundary. Insertion of the point P' splits Ω_P into two sub-volumes denoted by $\Omega_{P'}$ and ω_P as shown in figure 1.

The solution at node P' is obtained by solving a local finite element problem corresponding to the original equations on the elements surrounding the node P':

$$\begin{aligned}
&\int_\Omega \left\{ \rho\left(\frac{\partial \mathbf{u}}{\partial t} + \mathbf{u}\cdot\nabla\mathbf{u}\right) - \mathbf{f} \right\} \mathbf{v}_{P'} \mathrm{d}\Omega - \int_\Omega p(\nabla\cdot\mathbf{v}_{P'})\mathrm{d}\Omega \\
&\quad + \int_\Omega 2\mu\boldsymbol{\gamma}(\mathbf{u}) : \boldsymbol{\gamma}(\mathbf{v}_{P'})\mathrm{d}\Omega + \sum_K \int_{\Omega_K} \left\{ \rho\left(\frac{\partial \mathbf{u}}{\partial t} + \mathbf{u}\cdot\nabla\mathbf{u}\right) \right. \\
&\quad \left. + \nabla p - \nabla[2\mu\boldsymbol{\gamma}(\mathbf{u})] - \mathbf{f} \right\} \tau_u (\rho\mathbf{u}\cdot\nabla\mathbf{v}_{P'})\mathrm{d}\Omega_K \\
&\quad + \sum_K \int_{\Omega_K} (\nabla\cdot\mathbf{u})\delta(\nabla\cdot\mathbf{v}_{P'})\mathrm{d}\Omega_K = 0
\end{aligned} \tag{37}$$

$$\begin{aligned}
&\int_\Omega (\nabla\cdot\mathbf{u}) q_{P'} \mathrm{d}\Omega + \sum_K \int_{\Omega_K} \left\{ \rho\left(\frac{\partial \mathbf{u}}{\partial t} + \mathbf{u}\cdot\nabla\mathbf{u}\right) \right. \\
&\quad \left. + \nabla p - \nabla[2\mu\boldsymbol{\gamma}(\mathbf{u})] - \mathbf{f} \right\} \tau_u \nabla q_{P'} \mathrm{d}\Omega_K = 0
\end{aligned} \tag{38}$$

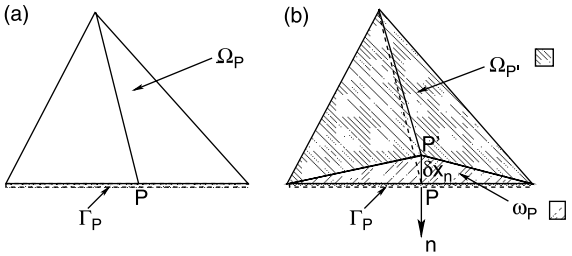

Figure 1. Extracting the normal derivative on boundary nodes: (a) element connectivity of boundary node P, (b) element connectivity of inserted node P'.

where $\mathbf{v}_{P'}$ and $q_{P'}$ denote the velocity and pressure test functions associated to the inserted node P'. We assume that the insertion of P' will not affect the values at the vertices of the patch Ω_P. Thus the only unknowns are the values of $\mathbf{u}$ and p at node P'. Once this local problem is solved, a finite difference between the values of the solution at the new node P' and boundary node P yields the normal derivative:

$$\frac{\partial \mathbf{u}}{\partial n}(\mathbf{x}_P) = -\frac{\mathbf{u}(\mathbf{x}_P + \delta \mathbf{x}_n) - \mathbf{u}(\mathbf{x}_P)}{\delta x_n} \tag{39}$$

In practice δx_n is chosen a few orders of magnitude smaller than the size of the element patch surrounding node P (10^{-4} to 10^{-3} of h_K; see Ilinca and Pelletier (2007) for details).

Finally, cartesian derivatives of the velocity are obtained by solving equations (33), (34) and (35). Because the gradient of the velocity is in the direction normal to the boundary this reduces to solving

$$\frac{\partial \mathbf{u}}{\partial x} = \frac{\partial \mathbf{u}}{\partial n} n_x \tag{40}$$

$$\frac{\partial \mathbf{u}}{\partial y} = \frac{\partial \mathbf{u}}{\partial n} n_y \tag{41}$$

$$\frac{\partial \mathbf{u}}{\partial z} = \frac{\partial \mathbf{u}}{\partial n} n_z \tag{42}$$

Additional accuracy is achieved if derivatives in equations (40), (41) and (42) are constrained to satisfy the continuity equation. This is done by, minimizing

$$J = \frac{1}{2}\left(\frac{\partial \mathbf{u}}{\partial \mathbf{x}} - \frac{\partial \mathbf{u}}{\partial n} n_{xyz}\right)^2 + l D^{\mathrm{T}} \frac{\partial \mathbf{u}}{\partial \mathbf{x}} \tag{43}$$

where $\mathrm{D}^{\mathrm{T}} = (1, 0, 0, 0, 1, 0, 0, 0, 1)$, l is the Lagrange multiplier associated to the incompressibility constraint and $\{\partial\mathbf{u}/\partial\mathbf{x}\}$, $\{(\partial\mathbf{u}/\partial n)n_{xyz}\}$ denote

$$\left\{\frac{\partial \mathbf{u}}{\partial \mathbf{x}}\right\}^{\mathrm{T}} = \left\{\frac{\partial u}{\partial x}, \frac{\partial u}{\partial y}, \frac{\partial u}{\partial z}, \frac{\partial v}{\partial x}, \frac{\partial v}{\partial y}, \frac{\partial v}{\partial z}, \frac{\partial w}{\partial x}, \frac{\partial w}{\partial y}, \frac{\partial w}{\partial z}\right\} \tag{44}$$

$$\begin{aligned}
&\left\{\frac{\partial \mathbf{u}}{\partial n} n_{xyz}\right\}^{\mathrm{T}} \\
&= \left\{\frac{\partial u}{\partial n} n_x, \frac{\partial u}{\partial n} n_y, \frac{\partial u}{\partial n} n_z, \frac{\partial v}{\partial n} n_x, \frac{\partial v}{\partial n} n_y, \frac{\partial v}{\partial n} n_z, \frac{\partial w}{\partial n} n_x, \frac{\partial w}{\partial n} n_y, \frac{\partial w}{\partial n} n_z\right\}
\end{aligned} \tag{45}$$

With this notation, minimization of the first term in the right handside of (43) leads to equations (40), (41) and (42), while minimization of the second term enforces the

incompressibility of the velocity field:

$$\mathrm{D}^{\mathrm{T}}\frac{\partial \mathbf{u}}{\partial \mathbf{x}} = \frac{\partial u}{\partial x} + \frac{\partial v}{\partial y} + \frac{\partial w}{\partial z} = 0 \tag{46}$$

The resulting system of equations is thus written as

$$\begin{bmatrix} \mathbf{I}_{9\times 9} & \mathrm{D} \\ \mathrm{D}^{\mathrm{T}} & 0 \end{bmatrix} \begin{Bmatrix} \dfrac{\partial \mathbf{u}}{\partial \mathbf{x}}_{l} \end{Bmatrix} = \begin{Bmatrix} \dfrac{\partial \mathbf{u}}{\partial n} n_{xyz} \\ 0 \end{Bmatrix} \tag{47}$$

with $\mathbf{I}_{9\times 9}$ the 9×9 identity matrix. The solution of the system (47) yields the derivatives of u, v, w consistent with $(\partial u/\partial x) + (\partial v/\partial y) + (\partial w/\partial z) = 0$. This values are used to evaluate the sensitivity boundary conditions.

4. Implementation

The flow and sensitivity equations are solved on 3D meshes. Time is discretized by an implicit Euler scheme and the equations are linearized with Newton's method. The solution algorithm works as follows:

- At each time step

- Iterate over the non-linear Navier–Stokes equations (12) and (13) until convergence. A few steps of successive substitution (Picard's method) are performed at the beginning of the first time step and the Newton's linearization is used afterward.
- Evaluate the solution gradient at the boundary and impose boundary conditions for the sensitivity equations.
- Use the matrix from the last Newton iteration on the flow problem and solve the linear system for the sensitivities equations (23) and (24). This step requires the evaluation of one right hand side and one linear equation solve for each parameter.

Element matrices are constructed using a numerical Jacobian technique and assembled in a compressed sparse row format. Flow and sensitivity global systems are solved by BiCG preconditioned iterative methods.

5. Numerical results

We consider the flow around a circular cylinder in ground proximity and study the effect of the ground to cylinder gap size s. The computational domain and boundary conditions are shown on figure 2. Because the problem is 2D a slab was meshed with one layer of tetrahedral elements. The mesh, shown on figure 3, was designed to provide adequate resolution for both the flow and its sensitivity. The inflow velocity U_0 is uniform. The initial conditions are obtained from a steady state solution of the flow and its sensitivities with respect to s. The Reynolds number $Re = \rho U_0 \mathrm{D}/\mu$ is set to 100.

5.1 Verification

As shown in Section 3, the Dirichlet boundary conditions for the flow sensitivity must be tangent to the cylinder surface. The values of the normal components of the sensitivities are then an indicator of the accuracy of Dirichlet sensitivity boundary conditions. Figure 4 shows the normal and tangential components of the sensitivity boundary condition. The variable on the x axis represents the angle θ measured counter clockwise from the rear stagnation point on the horizontal axis (ranges from 0 for the point $x = \mathrm{D}/2$, $y = 0$, to $\pi/2$ for $x = 0$, $y = \mathrm{D}/2$, and so on until 2π for $x = \mathrm{D}/2$, $y = 0$). As can be seen, the normal component of the sensitivity is very small and it is practically negligible when compared to the tangential component. This indicates that the method for recovering the flow gradients at the wall performs well.

Further verification is done by computing the flow sensitivities with respect to s by finite differences (FD). To this end, the distance to the ground s is changed by a small amount δs and the solution is recomputed. In order to minimize the influence of the mesh changes on the solution, the topology of the mesh is kept the same. Only nodes near the cylinder and found in the box $[-0.75D,$

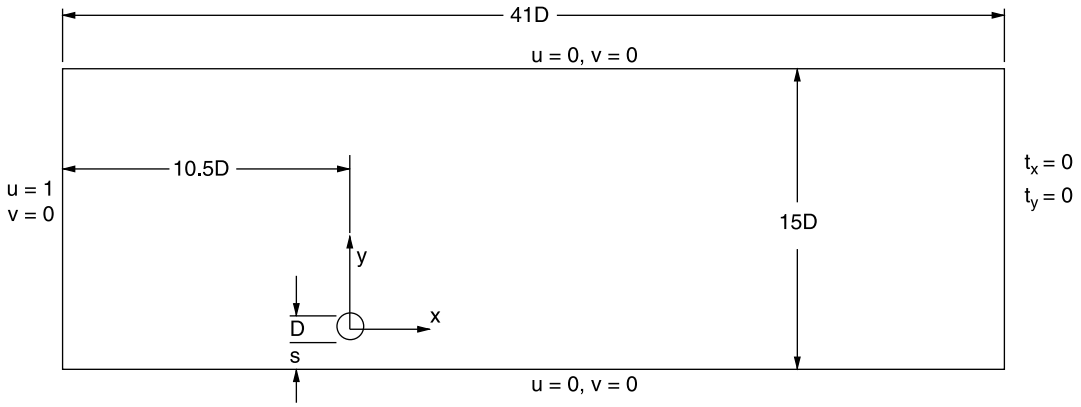

Figure 2. Flow around a circular cylinder in ground proximity: domain and boundary conditions.

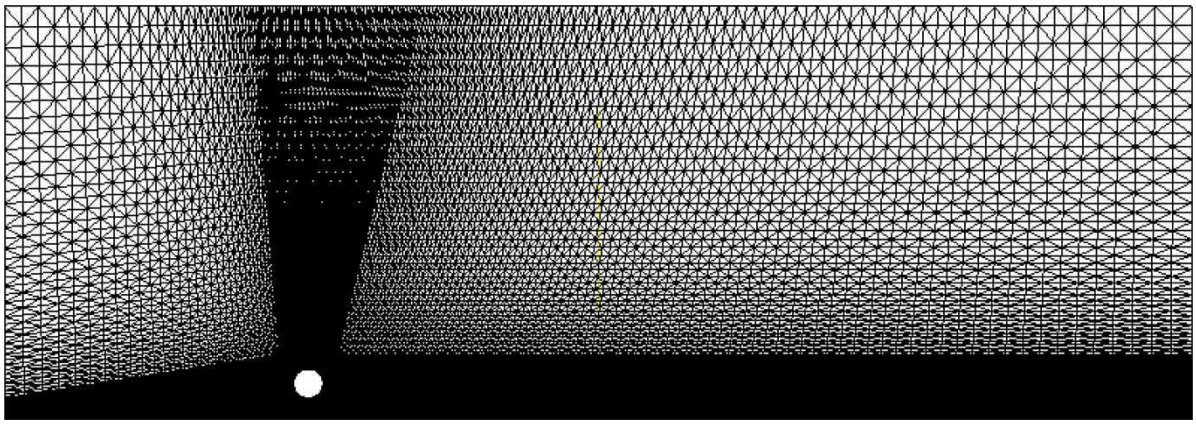

Figure 3. Mesh for the flow around a circular cylinder in ground proximity.

0.75D] × [−0.75*D*, 0.75D] are deplaced when changing s. The accuracy of the sensitivity is then verified at locations outside the subdomain where the nodes are allowed to move. Here we use points located at x = D, one diameter downstream of the centre of the cylinder. The reference finite difference flow sensitivity is determined from

$$\left(\frac{\partial \mathbf{u}}{\partial s}\right)_{\mathrm{FD}} = \frac{\mathbf{u}(s+\delta s) - \mathbf{u}(s-\delta s)}{2\delta s} \tag{48}$$

in which δs is taken very small compared to s. In this work we consider $\delta s = 0.001$D. The accuracy of the solution gradient from equation (48) is of the order $\mathcal{O}(\delta s^2)$.

Figure 5 compares the CSE predictions to FD approximations of s_u, s_v and s_p at x = D for steady state flow and $s = 0.75$D. As can be seen, the two sets of results agree extremely well indicating that the SEM performs well. It also indicates that the flow gradients are computed accurately at the Dirichlet boundary points.

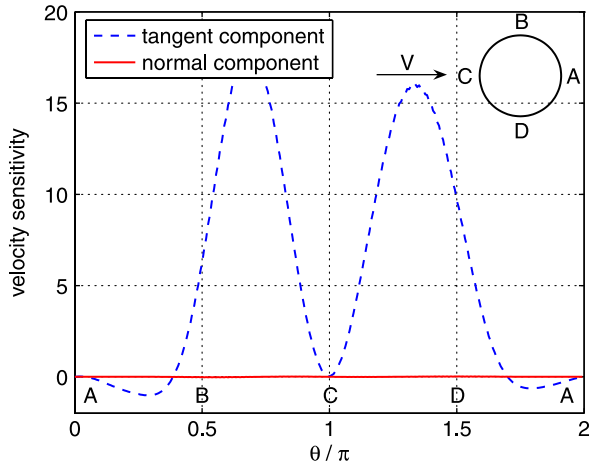

Figure 4. Components of the velocity sensitivity boundary condition on the cylinder surface.

5.2 *Sensitivity analysis of the unsteady flow*

The flow past a cylinder induces steady-state recirculating vortices for small gap values. When the distance to the wall increases above a critical value, vortex shedding is triggered behind the cylinder resulting in the well known Karman vortex street. We first look at results for the case s = D for which the vortex street develops rapidly. This is clearly seen on figure 6 which shows vorticity contours for times t = 104, 106, 108, and 110 (the time scale is set equal to D/U_0). To quantify the effect of the wall distance on the vortex street formation, simulations were also carried out for a gap size $s = 0.75$D. Vorticity contours are shown in figure 7 for t = 118–124, that is at latter times than for the case s = D (figure 6). As can be seen, the vortex street develops more slowly and with smaller amplitudes than for the case s = D. This is also seen in figure 8 which compares the time signal of the vertical velocity v at the point (x = 4D, y = D) for both cases.

Shape sensitivities with respect to the wall distance s were computed for $s = 0.75$D. The time signals at (x = 4D, y = D) for the flow and its sensitivities are shown in figure 9. The flow solution is shown in the left column of the figure. The SEM sensitivities are compared with a central finite difference approximation with $\delta s = 0.001$D (FD in figure 9). The following observations can be made:

- The periods of the sensitivity signals are the same as those of the flow;
- The amplitudes of the oscillation in sensitivities (s_u, s_v, s_p) are larger and increase at a faster rate than those of the flow;
- In all cases the SEM sensitivities agree very well with the finite difference approximation.

Figure 10 presents the time variations of the oscillation amplitude of the v component of velocity and that of its sensitivity. Both sets of data are plotted on a logarithmic scale. Note that the amplitude of the sensitivity signal is much larger and increases faster than that of the flow

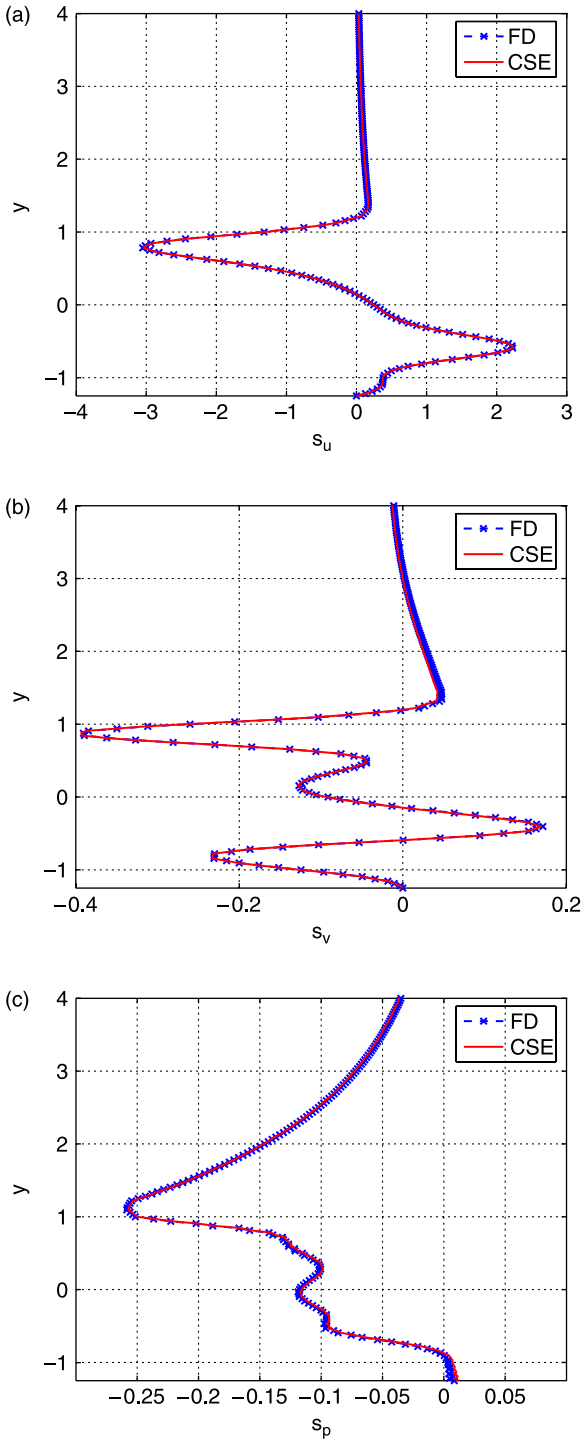

Figure 5. Steady state flow: verification of the computed sensitivity at $x = \mathrm{D}$.

solution. This is an important observation because it indicates that the sensitivities appear to be reacting faster and more strongly than the flow to changes in the parameter values. In other words, sensitivities appear able to foretell the transition from the steady-state solution to the vortex shedding before it becomes visible in the flow signal. This may prove very useful in flow control applications.

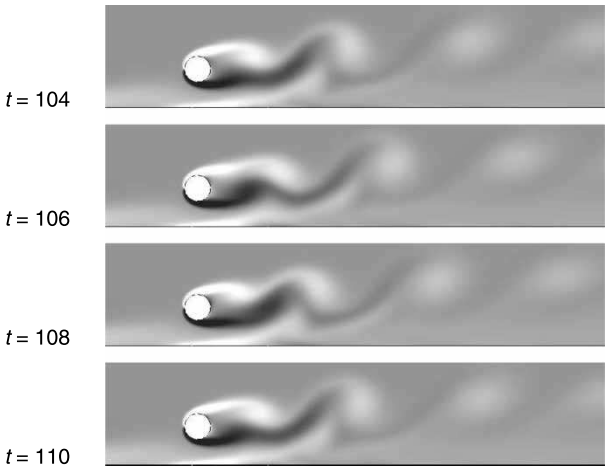

Figure 6. Flow around a circular cylinder at $s = \mathrm{D}$ from the wall: Von Karman vortex street.

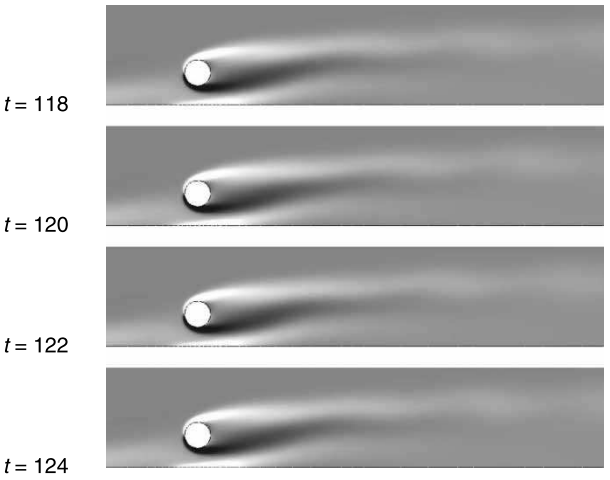

Figure 7. Flow around a circular cylinder at $s = 0.75\mathrm{D}$ from the wall: initiation of unstable flow.

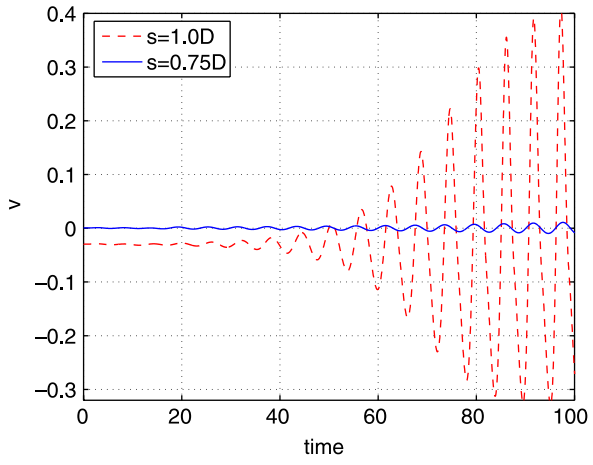

Figure 8. Time signal of the vertical velocity at ($x = 4\mathrm{D}$, $y = \mathrm{D}$).

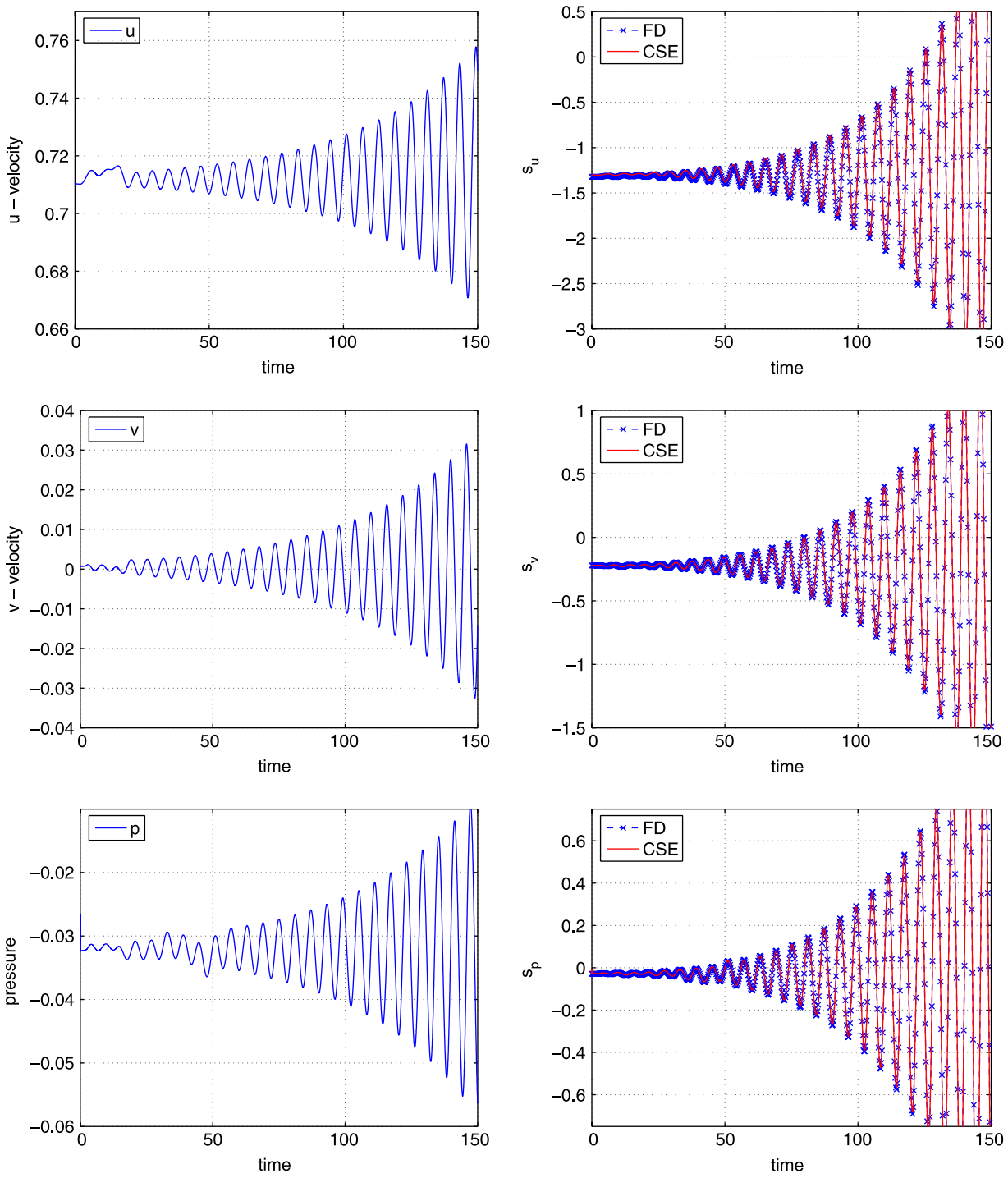

Figure 9. Time signal of the flow and its sensitivities with respect to s at ($x = 4$D, y = D) for $s = 0.75$D.

5.3 *Fast evaluation of flows on nearby geometries*

We now show how to use sensitivities for fast evaluation of flows on nearby geometries. Consider for example what happens to the u-velocity, when the gap parameter s is subject to a variation δs from its reference value s_0. First order Taylor series expansion in s yields:

$$u(x, y, z, t; s_0 + \delta s) \approx u(x, y, z, t; s_0) + \left.\frac{\partial u}{\partial s}\right|_{s_0} \delta s. \qquad (49)$$

Using the baseline solution obtained at $s = 0.75$D, we compare the flow estimates from the Taylor series for u and v to a full flow reanalysis at the perturbed values of the parameter, i.e. equation (49) vs $u(x,y,z,t;s_0 + \delta s)$. Results for two values of s, one lower ($s = 0.74$D) and the other larger ($s = 0.76$D) than the baseline value are shown in figures 11 and 12 for the point ($x = 4$D,y = D). Note that the location of this point relative to the ground is maintained unchanged when the ground to cylinder gap changes (i.e. the ground is kept fixed and the cylinder is deplaced).

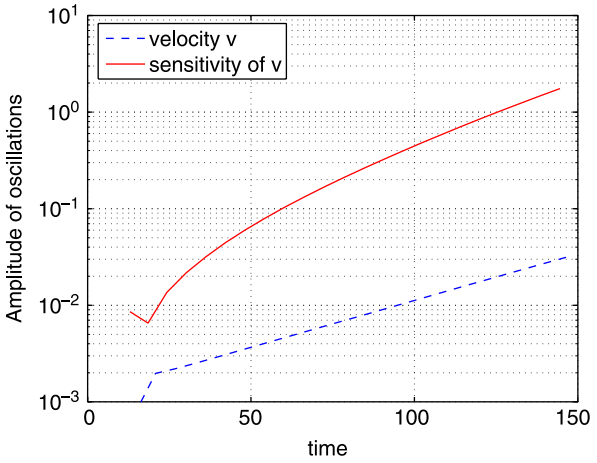

Figure 10. Amplitude of oscillations in v and its sensitivity at ($x = 4$D, $y = $ D) for $s = 0.75$D.

The reconstructed solutions are very close to those obtained by reanalysis at the perturbed value of s. The Taylor series approximations of the flow response are in very good agreement with the CFD reanalysis at early times. Agreement deteriorates very slightly at later times, probably because higher order derivatives in the Taylor series expansion become important. Observe also that sensitivities provide other quantitative information concerning trends of the flow response. They predict the damping of the vortex shedding when s decreases (figure 11) and the amplification of unsteadiness when the cylinder to ground gap increases (figure 12).

6. Conclusion

A general shape sensitivity equation formulation was developed for time-dependent incompressible laminar flows. The method is applied to the flow around a circular cylinder in proximity to the ground. Sensitivities are used to study the influence of the distance to the wall on the amplitude of vortex shedding behind the cylinder. The sensitivity of the flow is computed and correlated with the flow response when the wall distance changes. For $s = 0.75$D, the amplitudes of the sensitivity oscillations increase much faster with time than those of the flow. Hence sensitivities provide useful information to anticipate the flow response. The damping of vortex shedding

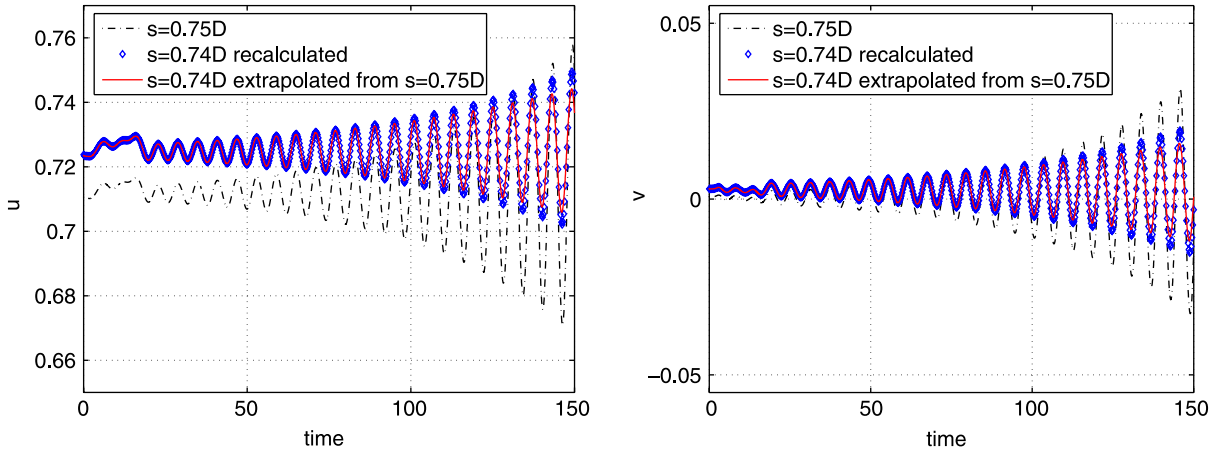

Figure 11. Flow at ($x = 4$D,$y = $ D): fast evaluation of flow at $s = 0.74$D from $s = 0.75$D.

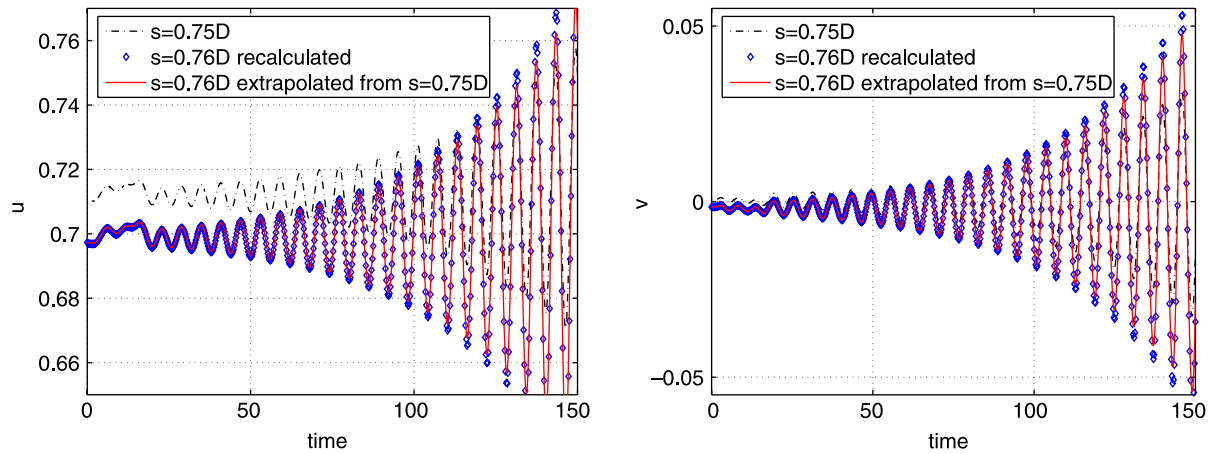

Figure 12. Flow at ($x = 4$D,$y = $ D): fast evaluation of flow at $s = 0.76$D from $s = 0.75$D.

with decreasing *s*/D is well predicted. Amplification of shedding with increased *s*/D is also well predicted. This property of sensitivities will likely prove useful in developing flow control algorithms to maintain certain characteristics of the flow (for example minimize the vortex street or added mass effects).

Acknowledgements

This work was sponsored in part by NSERC (Government of Canada), and by the Canada Research Chair Program (Government of Canada).

References

Blackwell, B.F., Dowding, K.J., Cochran, R.J. and Dobranich, D., Utilization of sensitivity coefficients to guide the design of a thermal battery. *Proceedings of the 1998 ASME/IMECE*, Anaheim, CA, HTD-Vol. 561–5, pp. 73–82, 1998.

Borggaard, J. and Burns, J., A PDE sensitivity equation method for optimal aerodynamic design. *J. Comp. Phy.*, 1997, **136**(2), 366–384.

Duvigneau, R. and Pelletier, D., Evaluation of nearby flows by a shape sensitivity equation method. *Proceedings of the 43th AIAA Aerospace Sciences Meeting and Exhibit*, Reno, NV, AIAA-2005–0127, 2005.

Duvigneau, R. and Pelletier, D., On accurate boundary conditions for a shape sensitivity equation method. *Int. J. Numer. Method Fluids*, 2006, **50**, 147–164.

Franca, L.P. and Frey, S.L., Stabilized finite element methods: II. The incompressible Navier–Stokes equations. *Comp. Methods Appl. Mech. Eng.*, 1992, **99**(2–3), 209–233.

Godfrey, A.G. and Cliff, E.M., Direct calculation of aerodynamic force derivatives: a sensitivity-equation approach. *Proceedings of the 36th AIAA Aerospace Science Meeting and Exhibit*, Reno, NV, AIAA Paper 98–0393, 1998.

Godfrey, A.G. and Cliff, E.M., Sensitivity equations for turbulent flows. *Proceedings of the 39th AIAA Aerospace Sciences Meeting and Exhibit*, Reno, NV, AIAA Paper 2001–1060, 2001.

Griewank, A., *Evaluating Derivatives*, 2000 (SIAM: Philadelphia, PA).

Gunzburger, M.D., *Perspectives in Flow Control and Optimization*, 2002 (SIAM: Philadelphia, PA).

Haug, E.J., Choi, K. and Komkov, V., Design sensitivity analysis of structural systems. *Mathematics in Science and Engineering*, Vol. 177, 1986 (Academic Press: Orlando).

Hien, T.D. and Kleiber, M., Stochastic finite element modeling in linear heat transfer. *Comput. Methods Appl. Mech. Eng.*, 1997, **144**, 111–124.

Hristova, H., Étienne, S., Pelletier, D. and Borggaard, J., A continuous sensitivity equation method for time-dependent incompressible laminar flows. *Int. J. Numer. Method Fluids*, 2006, **50**, 817–844.

Hughes, T.J.R., Franca, L.P. and Balestra, M., A new finite element formulation for computational fluid dynamics: V. circumventing the Babuka–Brezzi condition: a stable Petrov-Galerkin formulation of the Stokes problem accommodating equal-order interpolations. *Comp. Methods Appl. Mech. Eng.*, 1986, **59**, 85–99.

Hughes, T.J.R., Franca, L.P. and Hulbert, G.M., A new finite element formulation for computational fluid dynamics: VII. the Galerkin-least-squares method for advective-diffusive equations. *Comp. Methods Appl. Mech. Eng.*, 1989, **73**, 173–189.

Hughes, T.J.R., Engel, G., Mazzei, L. and Larson, M.G., The continuous Galerkin method is locally conservative. *J. Comp. Phys.*, 2000, **163**, 467–488.

Ilinca, F. and Pelletier, D., Computation of accurate nodal derivatives of finite element solutions: the finite node displacement method. *Int. J. Numer. Methods Eng.*, 2007, **71**, 1181–1207.

Ilinca, F., Hétu, J.-F. and Pelletier, D., On stabilized finite element formulations for incompressible advective-diffusive transport and fluid flow problems. *Comp. Meth. Appl. Mech. Eng.*, 2000, **188**(1–3), 235–255.

Ilinca, F., Hétu, J.-F. and Pelletier, D., Design sensitivity analysis for the optimization of the injection molding process. *Int. Polym. Proc.*, 2005, **20**, 86–92.

Ilinca, F., Pelletier, D. and Borggaard, J., A continuous second-order sensitivity equation method for time-dependent incompressible laminar flows. *Int. J. Numer. Method Fluids*, 2007, **55**(6), 565–587.

Limache, A., Aerodynamic Modeling Using Computational Fluid Dynamics and Sensitivity Equations. PhD Thesis, Virginia Polytechnic Institute and State University, Blacksburg, VA, 2000.

Lu, S.-Y. and Sagaut, P., Direct sensitivity analysis for smooth unsteady compressible flows using complex differentiation design. *Int. J. Numer. Methods Fluids*, 2007, **53**(12), 1863–1886.

Lyness, J.-N. and Moler, C.B., Numerical differentiation of analytic functions. *SIAM J. Numer. Anal.*, 1967, **4**(2), 202–210.

Martins, J.R.R.A., Stradza, P. and Alonso, J.J., The complex-step derivative approximation. *ACM T. Math. Software – TOMS*, 2003, **29**(3), 245–262.

Putko, M., Newman, P., Taylor, A. and Green, L., Approach for uncertainty propagation and robust design in CFD using sensitivity derivatives. *Proceedings of the 15th AIAA Comp. Fluid Dyn. Conf.*, Anaheim, CA, AIAA Paper 2001–2528, 2001.

Sherman, L.L., Taylor, A.C., III, Green, L., Newman, P.A., Hou, G.W. and Korivi, V.M., First- and second-order aerodynamic sensitivity derivatives via automatic differentiation. *J. Comp. Phys.*, 1996, **129**(2), 307–331.

Stanley, L.G. and Stewart, D.L., Design Sensitivity Analysis: Computational Issues of Sensitivity Equation Methods, *Frontiers in Applied Mathematics*, Vol. 25, 2001 (SIAM, Philadelphia).

Tezduyar, T.E., Shih, R., Mittal, S. and Ray, S.E., Incompressible flow using stabilized bilinear and linear equal-order-interpolation velocity-pressure elements, Research Report UMSI 90/165, University of Minnesota/Supercomputer Institute, Minneapolis, 1990.

Turgeon, É., Borggaard, J. and Pelletier, D., A continuous sensitivity equation approach to optimal design in mixed convection. *Numer. Heat Transf. A*, 2000, **38**, 869–885.

Turgeon, É., Pelletier, D. and Borggaard, J., Computation of airfoil flow derivatives using a continuous sensitivity equation method. *Proceedings of the 8th CASI Aerodynamics Symp.*, Toronto, Canada, 2001.

Turgeon, É., Pelletier, D. and Borggaard, J., A general continuous sensitivity equation formulation for complex flows. *Numer. Heat Transf. B*, 2002, **42**, 485–498.

Turgeon, É., Pelletier, D. and Borggaard, J., Application of continuous sensitivity equations to flows with temperature-dependent properties. *Numer. Heat Transf. A*, 2003, **44**(6), 611–624.

Turgeon, É., Pelletier, D. and Borggaard, J., A general continuous sensitivity equation formulation for the $k-\epsilon$ model of turbulence. *Int. J. CFD*, 2004, **18**, 29–46.

Zienkiewicz, O.C. and Zhu, J.Z., The superconvergent patch recovery and *a posteriori* error estimates. Part 1: the recovery technique. *Int. J. Numer. Methods Eng.*, 1992, **33**, 1331–1364.